

# Multiferroic behavior of Aurivillius $\text{Bi}_4\text{Mn}_3\text{O}_{12}$ from first-principles

Silvia Tinte

*INTEC-CONICET, Universidad Nacional del Litoral, Güemes 3450, (3000) Santa Fe, Argentina*

M. G. Stachiotti

*IFIR-CONICET, Universidad Nacional de Rosario,  
27 de Febrero 210 Bis (2000) Rosario, Argentina*

(Dated: June 25, 2018)

The multiferroic behavior of the hypothetical Aurivillius compound  $\text{Bi}_4\text{Mn}_3\text{O}_{12}$  has been explored on the basis of density functional calculations. We find that the tetragonal paraelectric phase of this material is ferromagnetic, showing ferroelectric and antiferrodistortive instabilities similar to the ones observed in its ferroelectric parent compound  $\text{Bi}_4\text{Ti}_3\text{O}_{12}$ . Our results indicate, however, that the presence of  $\text{Mn}^{+4}$  ions at the  $B$ -sites shrinks the cell volume and consequently the unstable polar mode, associated with the ferroelectric polarization, is overcome by an antiferrodistortive distortion. In this way,  $\text{Bi}_4\text{Mn}_3\text{O}_{12}$  exhibits incipient ferroelectricity at its equilibrium volume. We show that the ferroelectric state can be favored by strain or partial substitution of Mn with Ti.

PACS numbers: 77.84.-s, 75.85.+t, 63.22.Np

## I. INTRODUCTION

Multiferroic materials, exhibiting both ferroelectricity and magnetic order in the same phase, are of particular interest for their potential technological applications. One of the current trends in the search for new multiferroic compounds is, starting from a ferroelectric host, to incorporate magnetically active species and check whether it is (anti)ferromagnetic and insulating. An alternative way to predict multiferroic behavior is from material computational design, that is the prediction of multiferroic properties using first-principles techniques prior to their experimental verification.<sup>1-3</sup> Examples of this methodology include the prediction of a ferroelectric instability in  $\text{BiMnO}_3$ ,<sup>4</sup> several unstable phonon branches in  $\text{BiCrO}_3$ ,<sup>5</sup> structural instabilities of  $\text{CaMnO}_3$ <sup>6</sup> and the properties of as-yet-unsynthesized  $3d$ - $5d$  double perovskites.<sup>7</sup>

Between the ferroelectric materials, Aurivillius layered perovskites are good trials for multiferroics. Described by the formula  $[\text{Bi}_2\text{O}_2][\text{A}_{n-1}\text{B}_n\text{O}_{3n+1}]$ , they are formed by stacking fluorite blocks of  $\text{Bi}_2\text{O}_2$  with  $n$  perovskite-like blocks. Various  $A$  and  $B$  cations are allowed, so that this family has numerous representatives. Archetype compounds are  $\text{Bi}_2\text{WO}_6$  ( $n=1$ ),  $\text{SrBi}_2\text{Ta}_2\text{O}_9$  ( $n=2$ ) and  $\text{Bi}_4\text{Ti}_3\text{O}_{12}$  ( $n=3$ ). Recently some experimental groups have synthesized Aurivillius compounds incorporating magnetic ions at the  $B$ -site. The underlying idea was the substitution of magnetic transition metal cations into the central octahedron layer of the perovskite-type block, while maintaining ferroelectric displacements in the outer octahedron layers. For that reason, those works involved high-order Aurivillius phases ( $n>3$ ), such as  $\text{Bi}_5\text{Ti}_3\text{FeO}_{15}$ ,<sup>8-10</sup>  $\text{Bi}_6\text{Ti}_3\text{Fe}_2\text{O}_{18}$ ,<sup>10</sup> and  $\text{Bi}_5\text{Ti}_3\text{CrO}_{15}$ .<sup>11</sup> Sharma *et al.* reported ferroelectric behavior in a family of transition metal substituted three-layer Aurivillius phases, formulated  $\text{Bi}_{2-x}\text{Sr}_{2+x}(\text{Nb}/\text{Ta})_{2+x}\text{M}_{1-x}\text{O}_{12}$  ( $x \approx 0.5$ ,  $\text{M} = \text{Ru}^{4+}$ ,  $\text{Ir}^{4+}$  or  $\text{Mn}^{4+}$ ), showing that

these compounds have the same orthorhombic symmetry and similar dielectric and ferroelectric properties as their (non-magnetic) ferroelectric parent compounds.<sup>12,13</sup> Several investigations have been based on the incorporation of perovskite like  $\text{LaFeO}_3$ ,  $\text{BiMnO}_3$ , and  $\text{BiFeO}_3$  into a  $\text{Bi}_4\text{Ti}_3\text{O}_{12}$  matrix.<sup>14-16</sup> However, one can find that the reported magnetic properties in these materials are quite weak even at low temperature. The modification of  $\text{Bi}_4\text{Ti}_3\text{O}_{12}$  ceramics was also investigated by substituting their cations partly with Gd,<sup>17</sup> Fe,<sup>18</sup> and Mn.<sup>19</sup>

In spite of the large amount of experimental work showing that the generic structure of Aurivillius phases has the potential to serve as a template for multiferroic behavior, theoretical studies that help to clarify the effect of magnetic species in the Aurivillius structure are missing. In this paper we investigate the effects of the substitution of Ti ions by magnetically active  $\text{Mn}^{+4}$  ions at the  $B$  sites of  $\text{Bi}_4\text{Ti}_3\text{O}_{12}$  (BIT), which is a prototypical Aurivillius compound with bismuth also occupying the perovskite  $A$  site. BIT has received tremendous attention during the last decade, especially in the thin film form, due to its promise in nonvolatile ferroelectric random access memory applications.<sup>20</sup> It has a reasonably large spontaneous polarization ( $\sim 50 \mu\text{C}/\text{cm}^2$ ), a high Curie temperature (950 K), and fatigue resistance on Pt electrodes. Its complex crystal structure can be described in terms of relatively small perturbations from a high-symmetry body-centered tetragonal structure (space group symmetry  $\text{I4}/\text{mmm}$ ), which contains only one formula unit per primitive cell. Two main distortions from this tetragonal (paraelectric) structure lead to the ferroelectric orthorhombic phase. First, the ions displace along the  $[110]$  axis of the tetragonal structure. Second, the  $\text{TiO}_6$  octahedra rotate around the  $a$  and  $c$  axes.<sup>21</sup> The first distortion is directly responsible for the observed macroscopic polarization along the orthorhombic  $a$  direction ( $[110]$  axis of the tetragonal structure).

Specifically, we performed density-functional theory

calculations to investigate the hypothetical three-layer Aurivillius compound  $\text{Bi}_4\text{Mn}_3\text{O}_{12}$  (BIM), which results from substituting the three  $B$ -site  $\text{Ti}^{4+}$  cations with  $\text{Mn}^{4+}$  in the BIT lattice. We predict structural, electronic and magnetic properties of BIM, deepening the understanding of the effects of magnetic species in the Aurivillius structure of BIT. The paper is organized as follows. In Sec. II we describe computational details. Results are presented in Sec. III. Within this section we compare our BIM results with those of BIT from previous works and also with results we have obtained. First, the tetragonal structure of BIM is optimized and the electronic structure and magnetic order of this phase are discussed. Then we focus on the two more unstable modes of BIT: the zone-center  $E_u$  modes related to the polar instability and the zone-boundary  $X_3^+$  modes related to oxygen antiferrodistortive (AFD) distortions. We inspect then the energy landscape along the unstable modes directions and find that by replacing the Ti cations with Mn, the polar  $E_u$  mode is overcome by the  $X_3^+$  mode. Finally, we investigate the possibility of favoring the ferroelectric distortion by strain and chemical engineering.

## II. COMPUTATIONAL DETAILS

We performed standard first-principles calculations using density-functional theory within the generalized gradient approximation (GGA) with the Perdew, Burke and Ernzerhof<sup>25</sup> parametrization as implemented in the VASP-4.6 code.<sup>26</sup> The projector augmented wave potentials were used including explicitly 15 valence electrons for Bi ( $5d^{10} 6s^2 6p^3$ ), 13 for Mn ( $3p^6, 3d^5, 4s^2$ ), 10 for Ti ( $2p^6, 3d^3, 4s^1$ ) and 6 for oxygen ( $2s^2, 2p^4$ ). Convergence with respect to the  $k$ -point mesh was achieved using a  $6 \times 6 \times 6$   $\Gamma$ -centered grid. For a proper treatment of strongly localized Mn  $d$  electrons, we used the on-site Coulomb correction (GGA+ $U$ ) in the Dudarev implementation with parameter  $U_{eff} = U - J = 5.2$  eV.<sup>27</sup> Except for the calculations done to determine the magnetic ground-state, where different  $U_{eff}$  values were used to check the energy differences between spin configurations, all other calculations were performed using the mentioned value.

Using a 19-atom body-centered-tetragonal unit cell with space group  $I4/mmm$ , we relax all degrees of freedom (lattice parameters and internal coordinates along the stacking direction  $z$ ) for spin polarized structures. We optimized the ground state structures with a plane-wave cutoff of 600 eV which yielded good convergence and, hence, was also used for the rest of the calculations. To search for the presence of ferroelectric and antiferrodistortive instabilities in the tetragonal paraelectric structure, we determined the phonon frequencies and eigenvectors of the infrared-active  $E_u$  and rotational  $X_3^+$  modes, which are the main unstable modes of BIT. To this end, we calculated atomic forces of symmetry-adapted configurations determined with the help of the

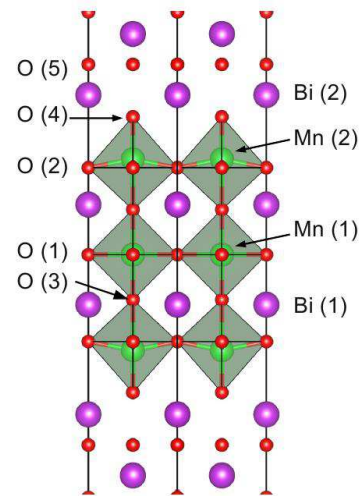


FIG. 1. (Color online) BIM tetragonal phase along  $[001]$  from 0 to  $c/2$ .

ISOTROPY software,<sup>28</sup> where selected atoms are displaced by  $0.01$  Å along the  $x$ ,  $y$  and/or  $z$  direction. To compute the  $X_3^+$  modes, in particular, the primitive cell was doubled to a 38-atom conventional tetragonal cell. From the forces as a function of displacements, a dynamical matrix of  $11 \times 11$  ( $8 \times 8$ ) for  $E_u$  ( $X_3^+$ ) symmetry was constructed and diagonalized. Once the eigenvectors have been determined, we evaluate the total energy as a function of the displacement pattern of the unstable (imaginary frequency) modes. Those curves will provide the ferroelectric and antiferrodistortive instability energy associated with a particular phonon mode.

## III. RESULTS

We begin by describing the optimized tetragonal structure of BIM. The minimized lattice parameters are  $a = 3.811$  Å and  $c = 32.613$  Å. These values are smaller than those we compute for BIT using GGA:  $a = 3.842$  Å and  $c = 33.241$  Å, which in turn differ slightly from the experimental values reported in the literature ( $a = 3.8633$  Å and  $c = 33.2942$  Å,<sup>29</sup> and  $a = 3.850$  Å and  $c = 32.832$  Å)<sup>21</sup>. As seen the replacement of  $\text{Ti}^{4+}$  ions with  $\text{Mn}^{4+}$  shrinks the equilibrium volume of the unit cell, which is consistent with the fact that six coordinated  $\text{Mn}^{4+}$  has an ionic radius ( $0.67$  Å) smaller than that of  $\text{Ti}^{4+}$  ( $0.745$  Å). This chemical substitution would be analogous to applying pressure on BIT and one could expect, following the general trend in many perovskite oxides, a strong sensitivity of the ferroelectric instability to volume.

In the perovskitelike blocks of the tetragonal structure, by symmetry there is one central  $\text{Mn}^{4+}$  ion [Mn(1) in Fig. 1] and two equivalent  $\text{Mn}^{4+}$  ions above and below the central layer, Mn(2). In the optimized structure of BIM,

TABLE I. Wyckoff positions for relaxed BIM tetragonal structure are compared to GGA calculations and experimental results for BIT.

Atom	Site	BIM	BIT	BIT exp. <sup>29</sup>
Bi1	e	0.4342	0.4336	0.4325
Bi2	e	0.2901	0.2887	0.2885
Mn1	a	0.0000	0.0000	0.0000
Mn2	e	-0.1254	-0.1275	-0.1293
O1	c	0.00000	0.0000	0.0000
O2	g	0.3858	0.3848	0.3823
O3	e	-0.0593	-0.0595	-0.0589
O4	e	-0.1810	-0.1815	-0.1817
O5	d	0.0000	0.0000	0.0000

the two Mn(2) cations are pushed away along the  $c$ -axis from the center of each oxygen octahedron towards the fluorite blocks. Besides, the oxygen octahedron around these Mn(2) ions are considerably elongated along the  $c$  axis, opposite to the undistorted central octahedron. The  $A$ -site  $\text{Bi}^{3+}$  ions [Bi(1)] also move towards the fluorite blocks, that is, they approach the O(2) ions, moving away from the O(1) ions. Table I lists the optimized internal atomic positions of BIM. For comparison, we include our GGA results for BIT and the respective experimental values from Ref. 29. As seen the internal coordinates in both compounds are similar.

The magnetic order of BIM was investigated by inspecting the total energy of different configurations with spin pointing along [001]. We have optimized separately the tetragonal structure for the ferromagnetic (FM) ordering and for the following antiferromagnetic (AFM) arrangements in the perovskitelike block:  $A$ ,  $C$ , and  $G$ -type, in which the fraction of parallel aligned first-neighbor spins is  $2/3$ ,  $1/3$ , and  $0$ , respectively. By comparing the total energy of those configurations we find that the magnetic ground state of the material is FM with local magnetic moments of  $3.3$  and  $3.4 \mu_B$  for Mn(1) and Mn(2), respectively, which are slightly higher than the formal value of  $3 \mu_B$  expected for a four-valence Mn ( $d^3$ ) atom. We find that the  $A$ -type AFM arrangement is located at an energy slightly higher than the FM state, just a few mRy/f.u. above it. The energy of the  $C$ -type AFM ordering is more separated,  $\sim 15$  mRy/f.u. above the FM state. Finally, the  $G$ -type AFM configuration lies a few mRy/f.u. above the  $C$ -type. It is known that the energy differences between spin configurations are directly related to the magnetic interactions or exchange constants, which depend on the on-site Coulomb repulsion parameter  $U_{eff}$ . Then, we have verified that the FM order is the most stable configuration for different choices of  $U_{eff}$ . Although the variation of  $U_{eff}$  produced quantitative changes, the hierarchy of the magnetic configurations is kept. We point out that the optimized crystal structure of BIM described above corresponds to the FM ground state. Furthermore, all of the following results have also been obtained using the FM spin configuration.

The total density of states (DOS) and projected DOS

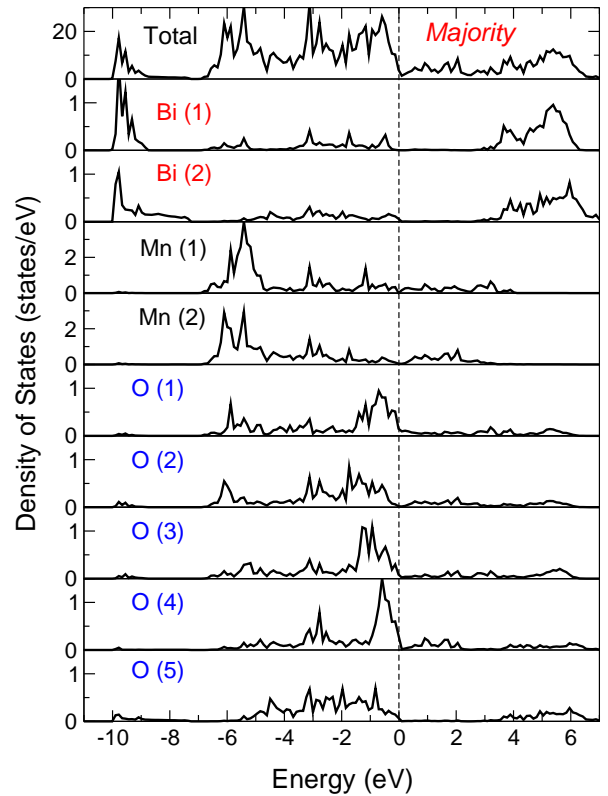


FIG. 2. Total majority-spin state and projected DOS onto atomic sites for tetragonal BIM. Zero energy is set as the Fermi level.

onto the atomic sites for the majority spins are shown in Fig. 2. The system has no band gap in the paraelectric  $I4/mmm$  phase, similar to what was observed for the paraelectric phase of other  $\text{AMnO}_3$  perovskites.<sup>4,30</sup> Instead, a half-metallic electronic structure is achieved with a band gap of  $\sim 2.2$  eV in the minority spins (not shown here). The occupied states of the conduction band (ranging from  $-7$  eV to the Fermi level) are mainly O  $2p$  and Mn  $3d$  states, which are strongly hybridized. The low-energy Bi states, around  $-10$  eV, come from the  $6s$  orbitals (the so-called lone pairs), while the unoccupied Bi  $6p$  states are located at high energies around  $6$  eV. The contribution of the Bi  $6s$  and  $6p$  states to the conduction band indicates that these states are hybridized with the  $2p$  of their neighbor oxygens, which is similar to what has been reported for BIT.<sup>22</sup> To better visualize the differences between BIM and BIT, the partial DOS of the  $B$ -site ion which is in an octahedron crystal field, are projected onto the  $t_{2g}$  and  $e_g$  orbitals (black lines and gray dashed areas in Fig. 3, respectively). The DOS of BIT was obtained at the BIM equilibrium crystal structure to avoid differences that could arise from the different lattice parameters of the two compounds. It is clear from the figure that the majority occupied Mn  $3d$  states are much more extended than those of Ti, showing that the Mn  $3d$  hybridize more strongly with the O  $2p$  states. The

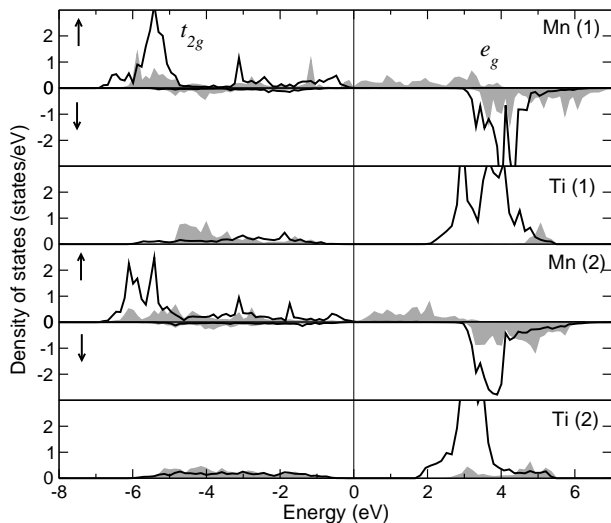


FIG. 3. DOS projected onto  $t_{2g}$  (black curves) and  $e_g$  (gray dashed regions) orbitals for each Mn site in BIM for the majority and minority spins. They are compared to the respective orbitals of the Ti cations in BIT. The DOS of BIT was computed at the BIM equilibrium volume.

majority-spin Mn  $t_{2g}$  states are fully occupied whereas the corresponding minority spins are practically empty. Concerning the  $e_g$  orbitals, the majority spins are more extended and they cross the Fermi level, which is responsible for the paraelectric phase being half-metallic.

Next we investigate the possibility of ferroelectricity in BIM by studying the unstable normal modes of the high-symmetry I4/mmm tetragonal phase, and compare our results with those for BIT. We note that as BIM is a hypothetical compound, we do not have an experimental low-temperature ground-state structure to decompose and identify the symmetry of active modes that would freeze in the high-temperature tetragonal phase. That limitation leads us to analyze the normal modes in tetragonal BIM with the same symmetry of the relevant modes found in the tetragonal parent compound BIT. Furthermore we are aware that the energy landscape of Aurivillius compounds, as it was shown in BIT<sup>23</sup> and SrBi<sub>2</sub>Ta<sub>2</sub>O<sub>9</sub>,<sup>24</sup> is much more complex than that of typical ferroelectric oxides, in which the freezing of one unstable polar mode directly explains the ferroelectric phase. So, based on an exhaustive study of the BIT phonon modes by Perez-Mato *et al.*,<sup>23</sup> we restrict our discussion to zone center polar modes with  $E_u$  symmetry and zone boundary antiferrodistortive modes with  $X_3^+$  symmetry. We find that two of the 11 bi-dimensional  $E_u$  modes of BIM have imaginary frequency, similarly to what was obtained for BIT.<sup>22,23</sup> The most unstable  $E_u$  mode [ $E_u(1)$ ,  $\omega = i146 \text{ cm}^{-1}$ ] involves primarily antiphase displacements of the Bi(1) ions with respect to the apical oxygen O(3), plus a smaller displacement of the central Mn(1) against its neighbor oxygens O(1). A similar pattern was indeed associated with the in-plane ferroelectric po-

larization of BIT.<sup>21</sup> The second unstable mode [ $E_u(2)$ ,  $\omega = i57 \text{ cm}^{-1}$ ] can be roughly described by the displacements of the Bi<sub>2</sub>O<sub>2</sub> layers relative to the perovskitelike blocks. This kind of instability was found in other Aurivillius family members,<sup>31</sup> and seems to be a general feature of them. Surprisingly, not only the eigenvectors but also the frequencies of the two unstable  $E_u$  modes are very similar to the ones obtained in a linearized augmented plane-wave (LAPW) calculation of BIT, where  $\omega = i145 \text{ cm}^{-1}$  and  $\omega = i48 \text{ cm}^{-1}$  were assigned for the  $E_u(1)$  and  $E_u(2)$  modes respectively.<sup>22</sup> Regarding the zone-boundary modes, the most unstable mode [ $X_3^+(1)$ ,  $\omega = i242 \text{ cm}^{-1}$ ], is much more negative than the polar  $E_u(1)$  mode. This mode takes place mainly at the center of perovskite slabs, tilting the central octahedron around the [110] direction,  $a^-a^-c^0$  in the Glazer notation. However, as the outer apical O(4) oxygens almost do not move, the two external octahedra are distorted. The second unstable AFD mode [ $X_3^+(2)$ ] consists mostly of the tilting of the two external octahedra around the [110] direction. This mode involves the displacement of the O(4) oxygens as well as the Bi(2) ions belonging to the fluorite layer. In summary, the described eigenvectors of the four unstable  $E_u$  and  $X_3^+$  modes are very similar to those obtained in BIT (illustrations of the different unstable eigenvectors of BIT are included in Ref. 23).

The energy landscape around the tetragonal structure as a function of the amplitude in Å of the unstable modes is shown in Fig. 4(a). For each mode, the eigendisplacement vector is normalized with respect to the tetragonal high-symmetry 38-atom unit cell. We summarize our results as follows. First, the most unstable  $X_3^+(1)$  mode decreases the total energy in  $\sim 21.4 \text{ mRy/f.u.}$ , against the  $\sim 7.5 \text{ mRy/f.u.}$  produced by the  $E_u(1)$  polar mode. This is strikingly different from what is observed in BIT where the rotational mode is overcome by the in-plane polar instability. With regard to the other two modes,  $X_3^+(2)$  and  $E_u(2)$ , they present a rather small energy instability. However, when each one by separate is combined with the most unstable mode of the same symmetry (open symbols), they further decrease the energy minimum of the double-well obtained with the most unstable mode. Interestingly, the particular an-harmonic coupling of  $X_3^+(2)$  with  $X_3^+(1)$  (open squares) yields an absolute energy minimum. The combination of these two rotational modes results in an atomic structure that differs from the high-symmetry phase mainly in that the central octahedron is slightly distorted and rotated around the [110] direction at an angle of  $\sim 10^\circ$ . This structure, however, is still half-metallic and ferromagnetic, as is the high-symmetry one. Finally, in Fig. 4(b) and 4(c), we explore the an-harmonic coupling between the two most unstable modes of different symmetry,  $X_3^+(1)$  and  $E_u(1)$ , to investigate whether they cooperate in the energy minimization. We find that the AFD  $X_3^+(1)$  distortion fully stabilizes the  $E_u(1)$  polar mode [open circles in Fig. 4(b)], when the last one is computed from the structure corresponding to the energy minimum of  $X_3^+(1)$ , compared to

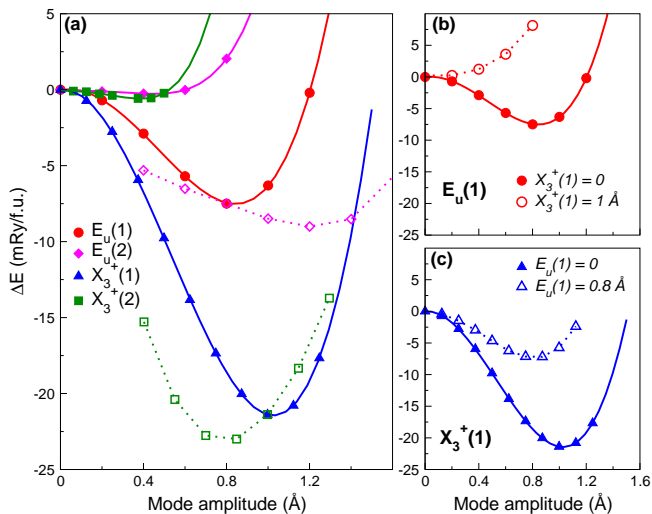


FIG. 4. (Color online) (a) Total energy per formula unit relative to the optimized tetragonal structure as a function of the unstable mode amplitudes with symmetry:  $X_3^+(1)$  (filled triangles and squares) and  $E_u(1)$  (filled circles and diamonds). Combination of same symmetry modes: less unstable mode  $X_3^+(2)$  (open squares) and  $E_u(2)$  mode (open diamonds) are superimposed to the energy minima of the most unstable mode,  $X_3^+(1)$  and ( $E_u(1)$ ), respectively. (b), (c) Coupling effect between the two most unstable modes of different symmetry. (b) Change of energy per f.u. as a function of the  $E_u(1)$  mode amplitude relative to a structure with mode  $X_3^+(1)$  frozen with amplitude of 1 Å (open circles). The curve for the pure  $E_u(1)$  distortion (filled circles) is repeated for comparison with. (c) Change of energy per f.u. as a function of the  $X_3^+(1)$  mode amplitude relative to a structure with mode  $E_u(1)$  frozen with amplitude of 0.8 Å (open triangles), and for the pure  $X_3^+(1)$  distortion (filled triangles).

TABLE II. BIM relaxed lattice parameter in the tetragonal structure at two different in-plane strains and in the equilibrium value.

In-plane strain	a (Å)	c (Å)
-2 %	3.7345	33.5498
0	3.8108	32.6128
+2 %	3.8870	32.0985

the pure  $E_u(1)$  distortion from the optimized tetragonal structure. Instead, the polar mode effect on the AFD  $X_3^+(1)$  [open triangles in panel (c)] is not so strong, but it does reduce the AFD double-well instability. Therefore, these behaviors indicate that the coupling of  $X_3^+(1)$  and  $E_u(1)$  is penalized.

Based on the existence of the polar instability in tetragonal BIM (although it is overcome by the rotational distortion), we investigate to what extent it would be possible to favor ferroelectricity by the application of epitaxial strain. We analyze two different structures around the equilibrium volume with in-plane lattice parameter,  $a_{+2\%}$  and  $a_{-2\%}$ . The lattice parameters obtained by fix-

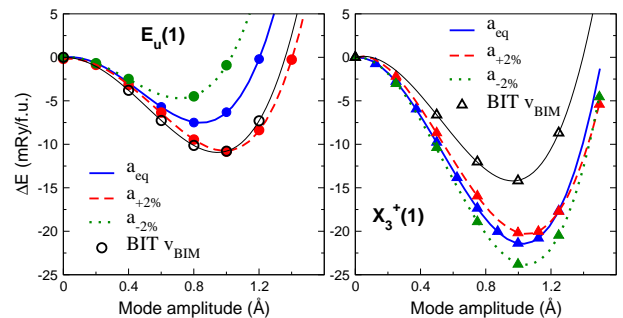


FIG. 5. (Color online) Effect of epitaxial strain on the two most unstable normal modes:  $E_u$  (left panel) and  $X_3^+$  (right panel). Energy differences relative to the optimized tetragonal structure for  $a_{eq}$  (filled lines),  $a_{+2\%}$  (dashed lines), and  $a_{-2\%}$  (dotted lines) using the eigenvectors obtained at the equilibrium volume. Open symbols correspond to BIT at the BIM equilibrium volume.

ing the in-plane lattice constants, and fully relaxing  $c$  and the atomic positions, are listed in Table II.

Figure 5 displays the energy landscape of the strained structures and compares them with the stress-free one. As expected, the in-plane  $E_u$  mode (left panel) is favored by tensile bi-axial strain, whereas the AFD  $X_3^+$  instability (right panel) is disfavored. This behavior, which is typical in  $ABO_3$  perovskite oxides, indicates that epitaxial strain seems to be an appropriate route to induce ferroelectricity in this Aurivillius compound. However, it can be estimated by extrapolating the above data that it is necessary to apply a strain of  $\sim +6\%$  to favor the polar mode over the antiferrodistortive distortion. This crudely estimated value is out of the range of strains usually accessible through epitaxial growth.

Since applying a large epitaxial strain is not easily achievable in practice, we instead explore the possibility of making BIM ferroelectric under a partial substitution of Mn by Ti. As a first test, we take the BIM equilibrium structure and replace all of the Mn ions with Ti; that is, we analyze BIT at the BIM equilibrium volume. The resulting energy curves are also plotted in Fig. 5 with open symbols. By comparing them with the BIM curves (filled lines), we see that effectively the presence of the Ti ions favors the polar instability and considerably decreases the AFD one. We can then speculate that a partial substitution of Mn with Ti would also favor ferroelectricity. To support this idea we check the energetics of the Aurivillius compounds  $Bi_4(TiMn_2)O_{12}$  with the  $B$  sites in the perovskitelike layer occupied by one Ti at the central octahedron, and two Mn ions in the external ones. We set the lattice parameters  $a$  and  $c$  by interpolating those values between the optimized BIM and BIT ones. We find that the polar mode  $E_u$  indeed is more unstable than the AFD one by  $\sim 3.8$  mRy/f.u., which shows that the Ti ion at the central octahedron plays an important role in stabilizing the ferroelectric mode over the AFD one. This is consistent with the fact that the

two modes of interest, as described above, are localized in the center of the perovskite slab. We think that this particular solid solution deserves a more detailed study in the future. Nevertheless, we can conclude that our results indicate that, not only the cell volume, but also the nature of the transition metal ion is indeed relevant for the stabilization of the ferroelectric phase in Aurivillius compounds. Therefore, it would be also interesting to further investigate the effect of magnetic species with higher ionic radius than  $\text{Mn}^{4+}$ , such as  $\text{Ru}^{4+}$  and  $\text{V}^{4+}$ .

In summary, we have investigated from first-principles the effects of magnetic Mn species in the Aurivillius structure of  $\text{Bi}_4\text{Ti}_3\text{O}_{12}$ . Specifically we explored the possibility of finding multiferroic behavior in the hypothetical Aurivillius compound  $\text{Bi}_4\text{Mn}_3\text{O}_{12}$ , which results from replacing the Ti with Mn ions. We have found that the paraelectric tetragonal structure of this material presents ferromagnetic order and structural instabilities similar to

BIT. We have shown, however, that the presence of Mn ions shrinks the cell volume, and the polar mode associated with the in-plane ferroelectric polarization, is overcome by an antiferrodistortive distortion. In this way,  $\text{Bi}_4\text{Mn}_3\text{O}_{12}$  exhibits incipient ferroelectricity at its equilibrium volume. We have seen that although it is possible to favor the polar state by the application of epitaxial strain, the necessary strain value is not easily achievable in practice. Our results indicate that the partial substitution of Mn with Ti is a fruitful alternative to favor the ferroelectric distortion, highlighting the relevant role played by the nature of the transition metal ion. We thus hope that our findings may be useful to better understand the multiferroic properties of Aurivillius compounds.

This work was supported by Grants No. PICT-PRH99 and No. PICT-2008(1867) from the ANPCyT-Argentina. M.G.S. gives thanks for financial support from Consejo de Investigaciones de la Universidad Nacional de Rosario.

- 
- <sup>1</sup> N. A. Spaldin and W. E. Pickett, *J. Solid State Chem.* **176**, 615 (2003).
  - <sup>2</sup> C. Ederer and N. A. Spaldin, *Curr. Opin. Solid State Mater. Sci.* **9**, 128 (2005).
  - <sup>3</sup> S. Picozzi and C. Ederer, *J. Phys.: Condens. Matter* **21** 303201 (2009).
  - <sup>4</sup> N. A. Hill and K. M. Rabe, *Phys. Rev. B* **59**, 8759 (1999).
  - <sup>5</sup> N. A. Hill, P. Baettig, and C. Daul, *J. Phys. Chem. B* **106**, 3383 (2002).
  - <sup>6</sup> S. Bhattacharjee, E. Bousquet, and P. Ghosez *Phys. Rev. Lett.* **102**, 117602 (2009).
  - <sup>7</sup> M. Lezaic and N. A. Spaldin, *Phys. Rev. B* **83**, 024410 (2011).
  - <sup>8</sup> X. Y. Mao, W. Wang, and X. Chen, *Solid State Commun.* **147**, 186 (2008).
  - <sup>9</sup> X. W. Dong, K. F. Wang, J. G. Wan, J. S. Zhu, J. Liu, J. Appl. Phys. **103**, 094101 (2008).
  - <sup>10</sup> A. Srinivas, S. V. Suryanarayana, G. S. Kumar and M. Mahesh Kumar, *J. Phys.: Condens. Matter* **11** 3335 (1999).
  - <sup>11</sup> A. T. Giddings, M. C. Stennett, D. P. Reid, E. E. McCabe, C. Greaves, N. C. Hyatt, *J. Solid State Chem.* **184**, 252 (2011).
  - <sup>12</sup> N. Sharma, B. J. Kennedy, M. M. Elcombe, Y. Liu and C. D. Ling, *J. Phys.: Condens. Matter* **20** 025215 (2008).
  - <sup>13</sup> N. Sharma, C. D. Ling, G. E. Wrighter, P. Y. Chena, B. J. Kennedy, and P. L. Lee, *J. Solid State Chem.* **180**, 370 (2007).
  - <sup>14</sup> Fei-Xiang Wu, Zhong Chen, Y. B. Chen, Shan-Tao Zhang, Jian Zhou, Yong-Yuan Zhu, and Yan-Feng Chen, *Appl. Phys. Lett.* **98**, 212501 (2011).
  - <sup>15</sup> X. Y. Mao, W. Wang, X. B. Chen, and Y. L. Lu, *Appl. Phys. Lett.* **95**, 082901 (2009).
  - <sup>16</sup> M. A. Zurbuchen, R. S. Freitas, M. J. Wilson, P. Schiffer, M. Roeckerath, J. Schubert, M. D. Biegalski G. H. Mehta, D. J. Comstock, J. H. Lee, Y. Jia, and D. G. Schlom, *Appl. Phys. Lett.* **91**, 033113 (2007).
  - <sup>17</sup> V. A. Khomchenko, G. N. Kakazei, Y. G. Pogorelov, J. P. Araujo, M. V. Bushinsky, D. A. Kiselev, A. L. Kholkin, and J. A. Paixo, *Mat. Lett.* **64**, 1066 (2010).
  - <sup>18</sup> X. Q. Chen, F. J. Yang, W. Q. Cao, H. Wang, C. P. Yang, D. Y. Wang, K. Chen, *Solid State Comm.* **150**, 1221 (2010).
  - <sup>19</sup> J. Ting and B. J. Kennedy, *J. Phys.: Conf. Ser.* **251**, 012029 (2010).
  - <sup>20</sup> J. F. Scott, *Ferroelectric Memories*, Springer Series in Advanced Microelectronics, Vol. 3 (Springer-Verlag, Berlin, 2000).
  - <sup>21</sup> A. D. Rae, J. G. Thompson, R. L. Withers, and A. C. Willis, *Acta Cryst., Sect. B: Struct. Sci.* **46**, 474 (1990).
  - <sup>22</sup> R. Machado, M. G. Stachiotti, R. L. Migoni, and A. H. Tera, *Phys. Rev. B* **70**, 214112 (2004).
  - <sup>23</sup> J. M. Perez-Mato, P. Blaha, K. Schwarz, M. Aroyo, D. Orobengoa, I. Etxebarria, and A. Garcia, *Phys. Rev. B* **77**, 184104 (2008).
  - <sup>24</sup> J. M. Perez-Mato, M. Aroyo, and Alberto Garcia, P. Blaha, K. Schwarz, and J. Schweifer, K. Parlinski, *Phys. Rev. B* **70**, 214111 (2004).
  - <sup>25</sup> J. P. Perdew, K. Burke, and M. Ernzerhof, *Phys. Rev. Lett.* **77**, 3865 (1996).
  - <sup>26</sup> G. Kresse and J. Hafner, *Phys. Rev. B* **47**, R558 (1993). G. Kresse and J. Furthmuller, *Phys. Rev. B* **54**, 11169 (1996).
  - <sup>27</sup> Note that as our hypothetical material prevents us from extracting  $U_{eff}$  from experiments, we have taken that value from the literature for  $\text{BiMnO}_3$  [Pio Baettig, Ram Seshadri, and Nicola A. Spaldin, *J. Am. Chem. Soc.* **129**, 9854 (2007)] since this oxide has a similar structure to the perovskitelike blocks of the Aurivillius compound.
  - <sup>28</sup> H. T. Stokes, D. M. Hatch, and B. J. Campbell, computer code ISOTROPY ([stokes.byu.edu/isotropy.html](http://stokes.byu.edu/isotropy.html)).
  - <sup>29</sup> C. H. Hervoches and P. Lightfoot, *Chem. Mater.* **11**, 3359-3364 (1999).
  - <sup>30</sup> N. Li, K.L. Yao, Z.Y. Sun, L.Zhu and G.Y. Gao *J. Appl. Phys.* **109**, 083715 (2011).
  - <sup>31</sup> M. G. Stachiotti, C. O. Rodriguez, C. Ambrosch-Draxl, and N. E. Christensen, *Phys. Rev. B* **61**, 14434 (2000).